

Early results from GLASS-JWST XV: the faintest red sources in the NIRCAM deep fields are intrinsically blue.

K. GLAZEBROOK ¹ T. NANAYAKKARA ¹ C. JACOBS ,^{1,2} N. LEETHOCHAWALIT ,^{3,4,5} A. CALABRÒ ,⁶ A. BONCHI,^{6,7} M. CASTELLANO ,⁶ A. FONTANA ,⁶ C. MASON ,^{8,9} E. MERLIN ,⁶ T. MORISHITA ,¹⁰ D. PARIS ,⁶ M. TRENTI ,^{3,4} T. TREU ,¹¹ P. SANTINI ,⁶ X. WANG ,¹⁰ K. BOYETT ,^{3,4} MARUSA BRADAC ,^{12,13} G. BRAMMER ,^{8,9} T. JONES ,¹³ D. MARCHESEINI ,¹⁴ M. NONINO ,¹⁵ AND B. VULCANI ,¹⁶

¹Centre for Astrophysics and Supercomputing, Swinburne University of Technology, PO Box 218, Hawthorn, VIC 3122, Australia

²ARC Centre of Excellence for All Sky Astrophysics in 3 Dimensions (ASTRO 3D), Australia

³School of Physics, University of Melbourne, Parkville 3010, VIC, Australia

⁴ARC Centre of Excellence for All Sky Astrophysics in 3 Dimensions (ASTRO 3D), Australia

⁵National Astronomical Research Institute of Thailand (NARIT), Mae Rim, Chiang Mai, 50180, Thailand

⁶INAF Osservatorio Astronomico di Roma, Via Frascati 33, 00078 Monteporzio Catone, Rome, Italy

⁷ASI-Space Science Data Center, Via del Politecnico, I-00133 Roma, Italy

⁸Cosmic Dawn Center (DAWN), Denmark

⁹Niels Bohr Institute, University of Copenhagen, Jagtvej 128, DK-2200 Copenhagen N, Denmark

¹⁰Infrared Processing and Analysis Center, Caltech, 1200 E. California Blvd., Pasadena, CA 91125, USA

¹¹Department of Physics and Astronomy, University of California, Los Angeles, 430 Portola Plaza, Los Angeles, CA 90095, USA

¹²University of Ljubljana, Department of Mathematics and Physics, Jadranska ulica 19, SI-1000 Ljubljana, Slovenia

¹³Department of Physics and Astronomy, University of California Davis, 1 Shields Avenue, Davis, CA 95616, USA

¹⁴Department of Physics and Astronomy, Tufts University, 574 Boston Ave., Medford, MA 02155, USA

¹⁵INAF-Trieste Astronomical Observatory, Via Bazzoni 2, 34124, Trieste, Italy

¹⁶INAF- Osservatorio astronomico di Padova, Vicolo Osservatorio 5, I-35122 Padova, Italy

(Received August 5th, 2022; Revised ??; Accepted ??)

Submitted to ApJL

ABSTRACT

We present a first look at the reddest 2–5 μ m sources found in deep NIRCAM images from the James Webb Space Telescope (JWST) GLASS Early Release Science program. We undertake a general search, i.e. not looking for any particular spectral signatures, for sources detected only in bands redder than reachable with the Hubble Space Telescope, and which are only marginally or not detected in bluer bands, corresponding to potential populations that may not have been identified before. We search for sources down to AB \sim 27 (corresponding to $> 10\sigma$ detection threshold) in any of the F200W, F277W, F356W or F444W filters, and demand a one magnitude excess with respect to all of the bluer bands (F090, F115W, F150W). Fainter than F444W > 25 we find 48 such sources. We fit photometric redshifts and spectral energy distributions to our 7-band photometry and identify the majority of this population ($\sim 70\%$) as $2 < z < 6$ galaxies that are faint at rest-frame ultraviolet-optical wavelengths, have stellar masses 10^8 – $10^9 M_\odot$, and have observed fluxes at $> 2\mu$ m boosted by a combination of the Balmer break and strong emission lines. Implied rest equivalent widths are $> 400\text{\AA}$. This is in contrast with brighter magnitudes where the red sources tend to be $z < 3$ quiescent galaxies and dusty star forming objects. The space density of $z \sim 4$ faint blue galaxies with high equivalent widths is an order of magnitude higher than found in pre-JWST surveys. Our general selection criteria allow us to independently identify other phenomena as diverse as the robust $z \sim 12$ Lyman Break Galaxy reported in paper III, and a very cool brown dwarf reported in XIII. In addition we discover an extremely low mass ($8 \times 10^8 M_\odot$) quiescent galaxy at $z \sim 2$, which is new uncharted territory for understanding the

regulation of star formation. This initial study – selecting objects ranging from extreme line emitters, passive galaxies, galaxies at $z > 11$ to brown dwarfs, demonstrates the power of JWST to discover and characterize new astronomical phenomena.

Keywords: editorials, notices — miscellaneous — catalogs — surveys. TODO

1. INTRODUCTION

The development of sensitive near-infrared areal detectors for astronomy led to the first sky surveys (Glazebrook et al. 1994) and the uncovering of new populations of high-redshift sources. The first large area imaging surveys discovered new populations of red objects, referred to early on as ‘Extremely Red Objects’ or ‘Distant Red Galaxies’ (McCarthy 2004; Franx et al. 2003); contrasting with the dominant population of ‘Faint Blue Galaxies’ (Ellis 1997). These redder objects were bright in the near-infrared but dim or undetected in the optical bands. These were later spectroscopically confirmed as mixture of $z \sim 2$ early type massive quiescent galaxies (McCarthy et al. 2004; Cimatti et al. 2004; Kriek et al. 2008), and massive dusty star-forming galaxies (Wuyts et al. 2009). These populations have now been photometrically and spectroscopically tracked to $z \sim 4$ (Marchesini et al. 2010; Spitler et al. 2014; Straatman et al. 2014; Marsan et al. 2015; Glazebrook et al. 2017; Schreiber et al. 2018; Forrest et al. 2020). The effects of quiescence, dust and redshift all add to make spectral energy distributions (SEDs) progressively redder in the optical to near-infrared bandpasses. In recent years, surveys have detected red $H - K$ and $H - 3.6\mu\text{m}$ sources that are likely even higher redshift quiescent and/or dusty sources (Merlin et al. 2019; Fudamoto et al. 2021; Marsan et al. 2022).

In the near-infrared the deepest surveys today come from the Hubble Space Telescope, however this is limited to wavelengths $< 1.6\mu\text{m}$. The state-of-the-art at longer wavelengths has been provided by the 85cm Spitzer Space Telescope which was retired in 2020. Now this is surpassed by new data from the James Webb Space Telescope (JWST; Rigby & et al. 2022) which has unprecedented capability at $2 - 5\mu\text{m}$ with the NIRCAM (Rieke et al. 2005) camera and $5 - 28\mu\text{m}$ with the MIRI camera (Rieke et al. 2015). Thus a first look at the sources that emerge in the longer wavelengths of JWST is a compelling prospect. In this paper we do this, utilising data from the GLASS Early Release Science program (Treu et al. 2022) where parallel imaging with NIRCAM provides extremely deep data at $2 - 5\mu\text{m}$, and our aim is to characterise the spectral energy distributions and possible nature and redshifts of these sources. In particular we adopt a complementary approach from other early JWST papers (Castellano et al. 2022, Paper III;

Leethochawalit et al. 2022, Paper X; Finkelstein et al. 2022; Atek et al. 2022; Donnan et al. 2022; Naidu et al. 2022; Yan et al. 2022); instead of searching for known classes of sources with particular color signatures we use a more general method which is sensitive to a wide variety of sources, and characterise what is revealed by the redder NIRCAM bands.

The plan of this paper is as follows: In 2 we describe the data and introduce the general method we use to select red sources. In section 3 we outline our analysis methodology including determination of redshifts, spectral types and stellar masses. In section 4 we discuss the nature of the population and their spectral energy distributions and likely redshifts. In section 5 we present conclusions. Throughout this paper we adopt AB magnitudes and a standard cosmology with $\Omega_m = 0.3$ $\Omega_\Lambda = 0.7$ and $H_0 = 70 \text{ km s}^{-1} \text{ Mpc}^{-1}$.

2. DATA AND SAMPLE SELECTION

GLASS-JWST is one of 13 Early Release Science programs. It obtained NIRISS and NIRSpec spectroscopy in the center of the massive $z = 0.31$ galaxy cluster A2744 on 28–29th June 2022, while obtaining NIRCAM images of two parallel fields 3–8 arcmin away from the cluster center. GLASS-JWST consists of the deepest extragalactic data amongst the ERS programs. Details can be found in the survey paper (Treu et al. 2022). For this paper we consider the NIRCAM parallel fields which are sufficiently distant from the cluster that only modest lensing magnification is expected (Medezinski et al. 2016). In this paper we neglect the effect, which does not affect colors, and the issue will be revisited after the completion of the campaign. The reduction of the images and construction of photometric catalogs are described in Merlin et al. (2022, Paper II). In summary we have seven filters covering $0.9 - 4.4 \mu\text{m}$ over an area of 9.7 arcmin^2 , with exposures of 1.6–6.5 hours, with the F444W filter being the deepest.

Our catalogue is F444W selected; the F444W image is the detection image and forced photometry is done in the other bands on images PSF-matched to F444W. We correct all bands to total based on the ratio of total to aperture flux in F444W. For this paper’s flux and color measurements we use an aperture of 0.45 arcsec (this is $3 \times$ the point spread function - PSF - full width half maximum in F444W). The 5σ limiting flux in F444W

for this aperture is 28.5, while the other six bands range from 28.1 to 27.6.

We aim to develop a general method to identify sources whose fluxes rise up in the redder bands. First we define the latter: for ‘red bands’ we utilise the F200W, F277W, F356W and F444W filters. Technically F200W is in the NIRCAM ‘short wavelength’ channel but for our purposes we include it in the ‘red band’ category as it represents a wavelength not accessible to HST and which is limited in depth by considerable thermal emission in ground-based observations. Then the ‘blue bands’ are F090W, F115W and F150W. We require a red selection that picks up a wide variety of sources and that at the faint end will pick up objects that are only marginally or not detected in the blue bands, but which at brighter magnitudes can be compared with previous HST+Spitzer work. After some experimentation we settled on the following:

1. We require that the photometry of a source be good in all 7 bands, i.e. no artefacts or chip boundaries affecting it which we determined by checking for flagged pixels near the source center. This removes 22% of all sources in the input sample.
2. We define a magnitude we call RED_BRIGHT, which is the brightest magnitude of a source in *any* of the red bands.
3. Next we similarly define BLUE_BRIGHT for the brightest of the blue bands.
4. We select $\text{RED_BRIGHT} - \text{BLUE_BRIGHT} > 1.0$
5. We examine the results as a function of the RED_BRIGHT magnitude limit.

This results in galaxies where at least one of the red bands is one magnitude brighter than *all of the blue bands*. This selection has several advantages: first it can pick up sources that are bright in only one red band (such as might be due to emission lines contributing at certain wavelengths) as well as continuum sources that are bright in many red bands. The $\text{RED_BRIGHT} - \text{BLUE_BRIGHT} > 1.0$ selection is defined in AB magnitudes, which is convenient as blue continuum sources such as star-forming galaxies have \sim constant AB magnitudes with wavelength, and our survey sensitivity is also \sim constant between bands (within a factor of two) in Janskies. Secondly by utilising a one magnitude break the red color selection is similar to previous methods that have been used to find high-redshift quiescent galaxies (e.g. [Straatman et al. 2014](#)), dusty galaxies ([Marchesini et al. 2010](#); [Spitler et al. 2014](#); [Franx et al. 2003](#))

and Lyman break galaxies ([Steidel et al. 2003](#)). Finally at the faint magnitudes it picks up sources undetected in the blue bands while at bright magnitudes it picks up previously known red populations.

We consider sources down to $\text{RED_BRIGHT} < 27.0$. At this magnitude limit the peak red fluxes in our aperture are $> 10\sigma$, which are robust sources. Also critically the blue limit for the faintest sources then corresponds to a $> 3\sigma$ detection, so we can be confident that the sources are reliably at $\text{RED_BRIGHT} - \text{BLUE_BRIGHT} \gtrsim 1$ even if not detected in the blue bands. One caveat to note is that by construction our catalog is F444W selected, with a point source completeness limit of 28.9 (Paper II). This translates to $\simeq 27.3$ for our aperture. Thus although a candidate may be bright in another red band it will always have some significant F444W flux. An advantage of F444W selection is that it probes out to $z = 7$ the rest frame optical where stellar mass-to-light ratios have smaller variation than in the rest frame ultraviolet. We ran a set of simple simulations (following the methodology of [Glazebrook et al. 2004](#) but with $z_{form} = 30$) using PEGASE.2 models ([Fioc & Rocca-Volmerange 1999](#)) and determined, that for maximally old galaxies, in the absence of significant amounts of dust obscuration, this corresponds to a strict stellar mass completeness limit of $6 \times 10^8 \text{ M}_\odot$ at $z = 3$ and $2 \times 10^9 \text{ M}_\odot$ at $z = 7$. Younger galaxies will be selected below these mass limits as they have lower mass-to-light ratios.

3. METHODOLOGY

We use v3.1 of the GLASS-ERS NIRCAM images and catalogues from Paper II, which contains 6590 sources. After selecting 7 bands of good photometry as noted above we have 5130 sources. Applying our $\text{RED_BRIGHT} - \text{BLUE_BRIGHT} > 1$ selection we have 162 sources¹ with $\text{RED_BRIGHT} < 27$. For these we fit the photometric redshifts and SEDs using the EAZY software ([Brammer et al. 2008](#)), specifically `ezay-py` version 0.5.2. Our EAZY fits use the ‘empirical’ template set `ezay_v1.3.spectra` which include high equivalent width emission line components which have proved important for fitting high-redshift sources ([Straatman et al. 2016](#)).

EAZY is a robust and accurate photometric redshift and multi-component SED fitting tool that has been utilised and validated in many deep surveys (e.g. [Straatman et al. 2016](#); [Whitaker et al. 2011](#); [Skelton et al. 2014](#)). However with only 7 near-infrared bands and a new telescope and instrument we approach it with cau-

¹ listed in Supplementary information online

tion and have inspected all of the SED fits in our faint sample. Inspection of this sample ($\text{RED_BRIGHT} > 25$; 67 objects) led to the further removal of 19 sources associated with image artefacts, blending with bright neighbours or chip edges. Of the remainder we find about 20% are bad fits, these are generally at the fainter end and have broad or multiply peaked redshift probability distributions ($P(z)$); however there are a handful of higher signal:noise object that simply can not be fit by EAZY. The majority, 80%, are excellent fits with the break between blue and red bands accurately recovered, with smoothly peaked redshift probability distributions. We interpret this high fraction as arising because breaks in photometry in general provide good photometric redshift constraints, and our sample includes these by construction. We caution that the reliability of photometric redshifts for sources outside our selection may be much less.

In Figure 1 we plot RED_BRIGHT vs photometric redshift for our sources and mark the typical limits of HST and Spitzer surveys. As a reference for this we take the Hubble Frontier Fields (HFF) depth from [Shipley et al. \(2018\)](#) which is the deepest near-infrared survey with HST. Their HST F160W point source completeness limit when corrected for our aperture corresponds to $\text{BLUE_BRIGHT} = 26.0$, we mark objects fainter than this in the blue channels with open circles. The Spitzer $3.6+4.5\mu\text{m}$ bands are similar to our F356W and F444W bands. In the HFF their depth was $\text{AB}=25$ (an aperture correction is inapplicable as Spitzer’s broad PSF makes faint objects effectively point sources). While there are significantly deeper Spitzer surveys they become seriously confusion limited and incomplete for $\text{AB} > 25$ (see Figure 14 of [Ashby et al. 2015](#)). This issue is normally addressed by modelling Spitzer fluxes using HST images as priors on source location, this introduces a dependence on detection in the bluer bands. Therefore we mark $\text{RED_BRIGHT}=25$ as the approximate limit for sources found with Spitzer, noting that Spitzer photometry of HST detected sources can go considerably deeper.

We use Prospector ([Johnson et al. 2021](#)) to derive stellar masses, star formation histories and dust attenuation for the galaxies in our sample because Prospector includes a physical treatment of the effect of emission lines on the photometry. We use a non-parametric `continuity_flex_sfh` with 4 SFH bins. We use a [Kroupa \(2001\)](#) IMF and fix the redshift of the galaxies at the best fit EAZY values. We use a [Calzetti et al. \(2000\)](#) dust law and let the dust optical depth vary between 0–2.0. We vary the stellar metallicity between $\log_{10}(\text{Z}/\text{Z}_\odot) = -2$ to 0.19. We further fix gas phase

metallicity to be same as stellar metallicity and allow the ionisation parameter of the galaxies to vary between $\text{U}=-1$ to -4 . We have inspected the Prospector SED fits and find them to agree well with the EAZY SED fits.

We define ‘quiescent galaxies’ as those with \log_{10} of the specific star-formation rate per year as < -9.4 . This is a factor of 4 below the main sequence at $3 < z < 4$ from [Schreiber et al. \(2018\)](#). We estimate dust attenuation A_V from the `dust2` parameter of the Prospector SED fits and code this in 3 bins on Figure 1. By inspecting the SEDs by eye we have verified that these attenuation classifications accord well with the shape and steepness of the best fit SEDs.

4. DISCUSSION OF SOURCES

Several trends are apparent in the source population. First it can be seen in Figure 1 that at bright magnitudes the sample is dominated by quiescent galaxies and dusty star forming galaxies at $z \sim 2$. This is a well known result as discussed in the introduction; and one might expect to see more such things at fainter magnitudes. However the nature of the population shifts and we see that at $\text{RED_BRIGHT} > 25$ the population is dominated ($\sim 70\%$) by low attenuation ($A_V < 1$) star forming galaxies at $2 < z < 6$. We also see candidate star-forming galaxies at $z > 11$ appearing, which we will discuss in detail later.

We present examples showing the ranges of sources at the faint end in Figure 2. ID numbers refer to the catalog of Paper II. To start with ID582 and ID1284 show examples of blue $z \sim 4$ star forming galaxies that are the dominant population of galaxies selected by our criteria. It can be seen that the increased flux $> 2\mu\text{m}$ comes from the Balmer break together with a strong contribution from $\text{H}\beta$ and $[\text{OIII}]$ emission lines. These SEDs can not be fit well at all without strong line flux contributions, if one removes the high equivalent width template from EAZY then the median χ^2 SED residual of the faint sample increases significantly from 2.2 to 7.7. The contribution of such emission lines can be seen in for example the F277 boost of ID582 and 1284 in Figure 1, it is even evident by eye in the F277 images.

The number of such sources was notable, so we investigated what level of emission line equivalent widths were needed to give such boosts to the photometry. To do this we measured the summed $\text{H}\beta + [\text{OIII}]$ 4959,5007Å equivalent widths of the best fit Prospector models. This confirms strong emission lines are needed and gives an indication of the level of line strengths required; the distribution is shown in Figure 3. It can be seen that very high equivalent widths are indicated with a rest-frame

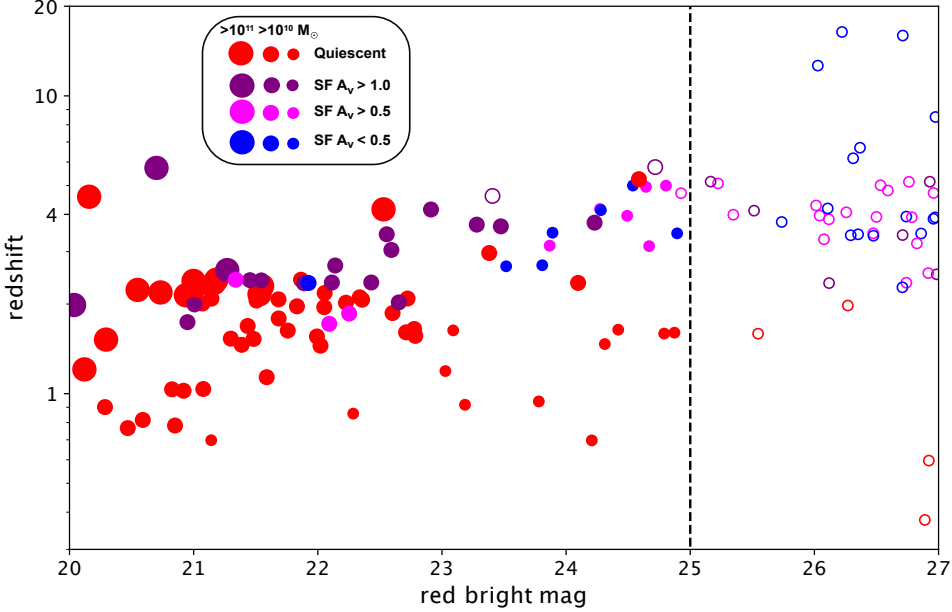


Figure 1. Redshift–magnitude distribution of the RED_BRIGHT–BLUE_BRIGHT > 1 selected sources. Symbol size and color are keyed to stellar mass, spectral type (quiescent/star forming) and dust attenuation as given in the legend. Open circles are the same coding, but denote objects that would be undetected in F160W in a deep HST survey, while the dashed vertical line shows the approximate Spitzer confusion limit.

range of 200–1400Å. This makes sense as the NIRCAM filters are quite broad, for example to boost the F277W by a factor of 50–70% (as shown by the SED ID 582 and 1284) requires an *observed* frame equivalent width of 3000–5000Å. The majority of the faint sample are low mass, we find the typical range of stellar mass is 10^8 – 10^9 M_\odot and the range of star formation rate from SED fitting (Prospector age < 100 Myr bin) is 1 – 4 M_\odot yr^{-1} . SED fitting is an unreliable method for measuring star formation rates; these values are likely underestimated given the equivalent widths and should be revisited by measuring emission line fluxes from spectra.

The high equivalent widths are in contrast with sources having bright magnitudes, where the median is ~ 80 Å for RED_BRIGHT < 25 . The implied equivalent width distribution is very similar to that identified at $1 < z < 3.4$ in our companion paper (Paper VI; [Boyett et al. 2022](#)) using NIRISS Wide Field Slitless Spectroscopy. We are sensitive to higher redshifts because NIRISS is limited to wavelengths $< 2\mu m$ whereas our selection by construction selects excess emission at $> 2\mu m$.

Objects with these kinds of extreme equivalent widths have been seen before, similarly selected via filter boosts (e.g., [Malkan et al. 2017](#)). For example at $z \sim 3$ [Forrest et al. \(2017\)](#) identified galaxies with equivalent widths

of ~ 800 Å by virtue of their excess in medium band filters. At higher redshift ($z > 7$) Spitzer photometry has indicated very high line emission boosts comparable to what we find (e.g. [Roberts-Borsani et al. 2020](#); [Skelton et al. 2014](#)). Such objects are interpreted as very young galaxies with high star formation rates but little stellar mass yet formed and are important to study due to their potential role in cosmic reionization at $z > 7$. The space density we find at $2 < z < 6$ is high, $\sim 2 \times 10^{-4}$ Mpc^{-3} for equivalent widths > 400 Å and RED_BRIGHT > 25 , a factor of ~ 7 higher than [Forrest et al. \(2017\)](#); although we note we are probing to considerably fainter magnitudes, hence lower stellar masses, and higher redshifts. Compared to all galaxies in NIRCAM with the same magnitudes they are $\sim 1\%$ of the population. We also find that compared to all $2 < z < 6$ galaxies in the entire NIRCAM sample they are about $\sim 2\%$ though we caution we have not validated the photometric redshifts for the broader sample.

ID1826 shows an example of a dustier star forming galaxy at $z \sim 4$ with $A_V = 1.3$, these are less common in the faint sample. Examples of even rarer selected sources are shown on the lower panels. ID5029 is well fit by a $z = 2.0$ quiescent galaxy with an extremely low stellar mass of 8×10^8 M_\odot , star formation rate $\lesssim 0.3$ M_\odot yr^{-1} and with moderate dust attenuation ($A_V = 1.3$).

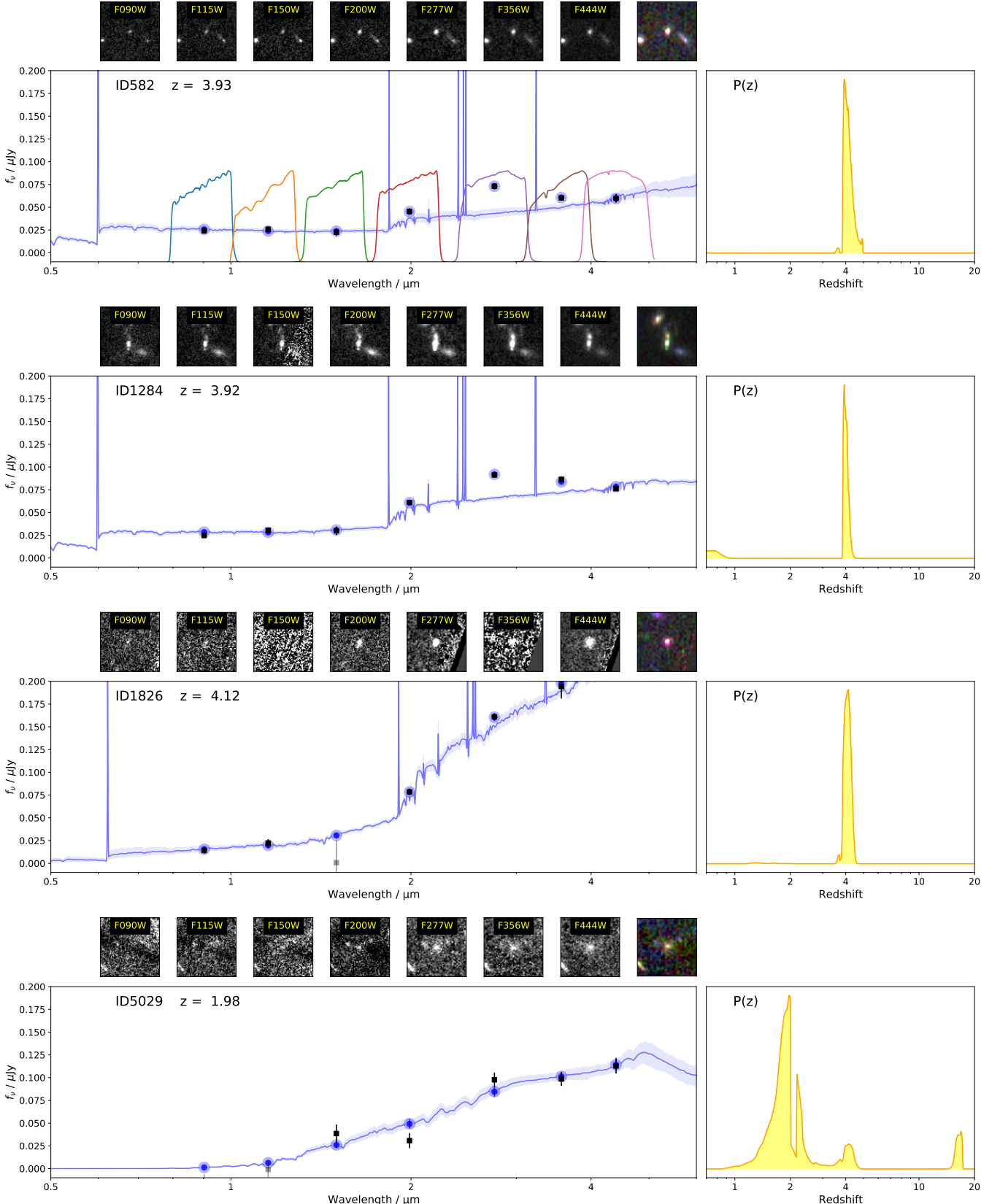


Figure 2. Image montages and EAZY SED fits of example objects. As well as the individual bands we show a ‘wide’ RGB color image constructed from F444W, F356W and F200W. The black points in the SED plots show the observed photometry, the blue line shows the best SED fit with the blue shading representing the template uncertainty. The large blue points are the best fit SED photometry. $P(z)$ probability distributions are shown for the SED fits in the right panels. In the top plot the NIRCAM filter transmission profiles are plotted to show their extent.

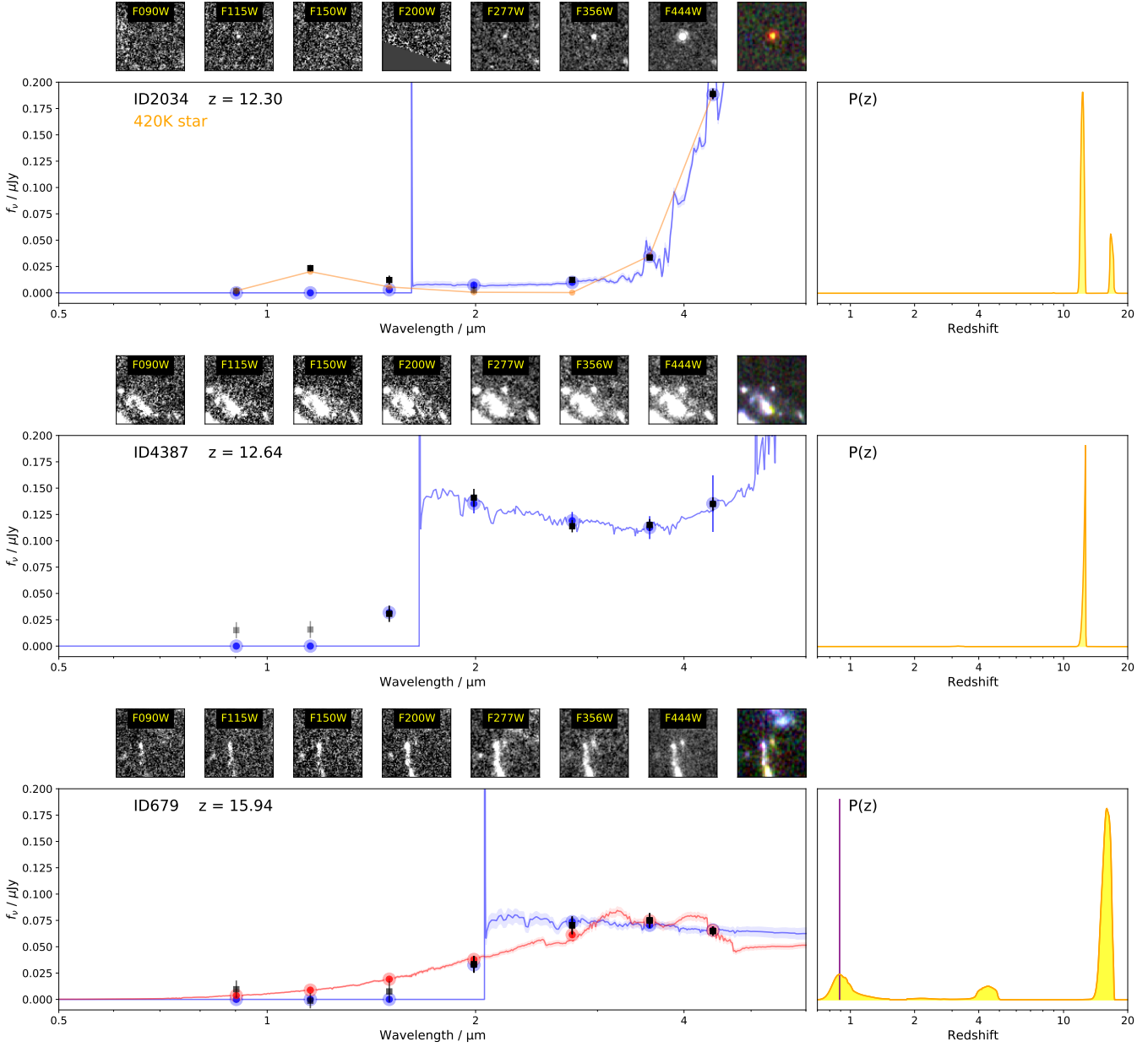


Figure 2. (contd.) Image montages and EAZY SED fits of further sources. ID2034 is significantly better fit by a ultra cool stellar spectrum (shown as the orange curve) rather than a high-redshift galaxy. We show two $z > 11$ Lyman break galaxy candidates. ID4387 is a strong candidate (Castellano et al. 2022), ID679 is a fainter, possible $z = 15.9$ galaxy. The alternate low-redshift $z = 0.89$ solution is also shown for the latter as a comparison (the second peak is marked on the $P(z)$ plot).

We expect such low mass quiescent galaxies to be significantly rarer than their massive cousins (of which many examples can be seen at brighter magnitudes in Figure 1) because the quiescent $z \sim 2$ galaxy stellar mass function of Tomczak et al. (2014) declines at low masses. However we note that this mass function is significantly incomplete below $3 \times 10^9 M_\odot$. The source is resolved with an estimated size of 0.2–0.4 arcsec; this is similar to those of the lowest mass ($\sim 10^{10} M_\odot$) quiescent galaxies of Nedkova et al. (2021). ID5029 is likely the lowest mass quiescent galaxy identified at $z \sim 2$. We note it has $F200W = 27.7$, considerably below the limit of ground based K -band surveys (Straatman et al. 2016). In a companion paper (Paper IX; Marchesini et al. 2022) we present the first spectra from JWST of two low mass ($\sim 10^{10} M_\odot$) quiescent galaxies. These results augur well for the future prospects of JWST to measure the properties of quiescent galaxies at low masses.

ID2034 is a point source and has an unusual SED with a strong rise between $F345W$ and $F444W$; the residual flux in $F115W$ strongly rules out a $z > 10$ solution. It is much better fit by a cool star, using the Phoenix stellar templates built in to EAZY we find a 400K Y dwarf is an excellent fit. This demonstrates how important it is to consider cool star templates when evaluating very high redshift solutions. We explore this object in more detail in our companion Paper XIII (Nonino et al. 2022) – which describes the independent discovery – with a more sophisticated set of stellar templates and conclude it is a star on the T/Y boundary. It is the first ultra cool dwarf to be discovered by JWST, its faint magnitude places it well outside the Milky Way thin disk.

ID4387 is a high confidence $z = 12.6$ Lyman break galaxy candidate with a pronounced Lyman dropout between $F150W$ and $F200W$, this was presented in detail in our companion Paper III (Castellano et al. 2022) where it was discovered by classical Lyman break color selection. We note the other bright galaxy in that paper at $z = 10.6$ is too low redshift to be selected by our method here; it has too much flux in $F150W$. Our method is not sensitive to Lyman break galaxies with redshifts $7 < z < 11$ as they have strong rest-ultraviolet continuum in the blue bands.

ID679 is a possible $z = 15.9$ Lyman break galaxy candidate with $F444W = 26.9$; it has a candidate Lyman break between $F200W$ and $F277W$, a blue continuum shape at longer wavelengths ($> 2\mu\text{m}$), and no flux detected in the bluer channels. It is quite faint; because of this the $F115W$ – $F200W$ color is not constrained well enough to have put it in the color selection window for these redshifts of Paper III. This also means the $z = 15.9$ solution is not robust; the SED and $P(z)$ of

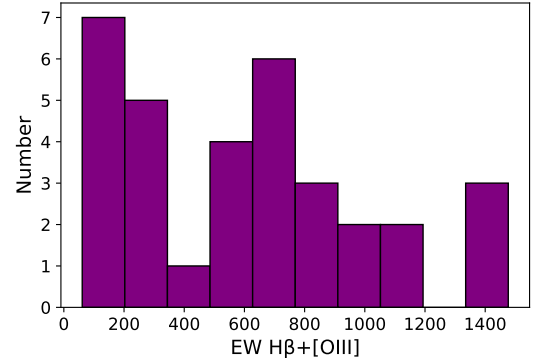


Figure 3. Photometrically inferred emission line ($H\beta + [OIII]$ 4961, 5007 Å) equivalent widths of Prospector fits to objects in our selected sample with $RED_BRIGHT > 25$ and $2 < z < 6$.

of this object show that there is significant probability of low redshift ($z \sim 1$). We show this alternate solution in the figure. Given low redshift is a priori more likely we can not regard this as a strong candidate. The other $z = 16.4$ object in Figure 1, ID2060, is similar and also has low- z solutions, furthermore it lies very close to the diffraction spike of a nearby bright galaxy that may contaminate the photometry. The discovery of $z \sim 16$ $F150W$ dropouts has attracted a lot of recent attention (Finkelstein et al. 2022; Donnan et al. 2022; Atek et al. 2022) and is scientifically important for our understanding of early galaxy formation, however as seen here SEDs at these redshifts may be ambiguous unless they have very high signal:noise (e.g., Zavala et al. 2022). Confirming the two objects in our sample would require significantly deeper imaging data, shortwards of $F200W$. These results do however indicate that our technique is a promising alternative to traditional methods to discover more of the very high-redshift objects.

5. CONCLUSIONS

We make a first exploration of the deep sky considering the faintest very red sources that emerge at wavelengths $> 2\mu\text{m}$ in JWST NIRCAM bands. Such sources would not have been seen by previous surveys. We utilise a novel general search method that does not depend on any particular choice of SED class to search for. We find 48 sources ($\sim 5 \text{ arcmin}^{-2}$) that are detected in one or more bands beyond $2\mu\text{m}$ but are absent or only marginally detected in bluer bands. Our primary conclusions are:

1. Our novel selection method picks out a diversity of different classes of interesting sources.

2. Contrary, perhaps, to a naive intuition, the population is dominated by low mass faint blue galaxies at $z \sim 4$, where the Balmer break and high equivalent width $\text{H}\beta + [\text{OIII}]$ emission lines are redshifted into the red bands. Such objects are more numerous than uncovered by pre-JWST surveys.
3. We find a few exotica such as a cool and distant T dwarf star and a very low mass quiescent galaxy at $z = 2$.
4. We recover a robust $z = 12.6$ Lyman break galaxy found by earlier color selection and identify two additional, weaker, candidates at $z \sim 16$. However, these two are not robust due to their very faint magnitudes. Nevertheless, this shows that our method has the potential to be a useful alternative to classical techniques in such searches.

The uncovering of new populations of galaxies in the red channels show the promise of JWST data for fully characterising the population of high-redshift galaxies and of stars in our galaxy. This analysis is only a preliminary first look to see what is revealed by red NIRCAM channels. Future work can greatly improve the statistics utilising future improved NIRCAM calibrations and deeper and wider JWST surveys. NIRCAM slitless spectroscopy ought to be able to quickly confirm the existence of an abundant $z \sim 4$ population of strong line emitters. Finally, it would be valuable

to add mid-infrared data from MIRI to better characterise the full SED shapes of the reddest objects that JWST/NIRCAM will find.

ACKNOWLEDGMENTS

This work is based on observations made with the NASA/ESA/CSA James Webb Space Telescope. The data were obtained from the Mikulski Archive for Space Telescopes at the Space Telescope Science Institute, which is operated by the Association of Universities for Research in Astronomy, Inc., under NASA contract NAS 5-03127 for JWST. These observations are associated with program JWST-ERS-1324. We acknowledge financial support from NASA through grants JWST-ERS-1342. KG, TN and CJ acknowledge support from Australian Research Council Laureate Fellowship FL180100060. NL and MT acknowledge support by the Australian Research Council Centre of Excellence for All Sky Astrophysics in 3 Dimensions (ASTRO 3D), through project number CE170100013. CM acknowledges support by the VILLUM FONDEN under grant 37459. The Cosmic Dawn Center (DAWN) is funded by the Danish National Research Foundation under grant DNRF140. MB acknowledges support from the Slovenian national research agency ARRS through grant N1-0238.

REFERENCES

Ashby, M. L. N., Willner, S. P., Fazio, G. G., et al. 2015, *ApJS*, 218, 33, doi: 10.1088/0067-0049/218/2/33

Atek, H., Shuntov, M., Furtak, L. J., et al. 2022, arXiv e-prints, arXiv:2207.12338. <https://arxiv.org/abs/2207.12338>

Boyyett, K., Mascia, S., Pentericci, L., et al. 2022, arXiv e-prints, arXiv:2207.13459. <https://arxiv.org/abs/2207.13459>

Brammer, G. B., van Dokkum, P. G., & Coppi, P. 2008, *ApJ*, 686, 1503, doi: 10.1086/591786

Calzetti, D., Armus, L., Bohlin, R. C., et al. 2000, *ApJ*, 533, 682, doi: 10.1086/308692

Castellano, M., Fontana, A., Treu, T., et al. 2022, arXiv e-prints, arXiv:2207.09436 (Paper III). <https://arxiv.org/abs/2207.09436>

Cimatti, A., Daddi, E., Renzini, A., et al. 2004, *Nature*, 430, 184, doi: 10.1038/nature02668

Donnan, C. T., McLeod, D. J., Dunlop, J. S., et al. 2022, arXiv e-prints, arXiv:2207.12356. <https://arxiv.org/abs/2207.12356>

Ellis, R. S. 1997, *Annual Review of Astronomy and Astrophysics*, 35, 389, doi: 10.1146/annurev.astro.35.1.389

Finkelstein, S. L., Bagley, M. B., Arrabal Haro, P., et al. 2022, arXiv e-prints, arXiv:2207.12474. <https://arxiv.org/abs/2207.12474>

Fioc, M., & Rocca-Volmerange, B. 1999, arXiv e-prints, astro. <https://arxiv.org/abs/astro-ph/9912179>

Forrest, B., Tran, K.-V. H., Broussard, A., et al. 2017, *ApJL*, 838, L12, doi: 10.3847/2041-8213/aa653b

Forrest, B., Marsan, Z. C., Annunziatella, M., et al. 2020, *ApJ*, 903, 47, doi: 10.3847/1538-4357/abb819

Franx, M., Labb  , I., Rudnick, G., et al. 2003, *ApJL*, 587, L79, doi: 10.1086/375155

Fudamoto, Y., Oesch, P. A., Schouws, S., et al. 2021, *Nature*, 597, 489, doi: 10.1038/s41586-021-03846-z

Glazebrook, K., Peacock, J. A., Collins, C. A., & Miller, L. 1994, MNRAS, 266, 65, doi: 10.1093/mnras/266.1.65

Glazebrook, K., Abraham, R. G., McCarthy, P. J., et al. 2004, Nature, 430, 181, doi: 10.1038/nature02667

Glazebrook, K., Schreiber, C., Labb  , I., et al. 2017, Nature, 544, 71, doi: 10.1038/nature21680

Johnson, B. D., Leja, J., Conroy, C., & Speagle, J. S. 2021, ApJS, 254, 22, doi: 10.3847/1538-4365/abef67

Kriek, M., van Dokkum, P. G., Franx, M., et al. 2008, ApJ, 677, 219, doi: 10.1086/528945

Kroupa, P. 2001, MNRAS, 322, 231, doi: 10.1046/j.1365-8711.2001.04022.x

Leethochawalit, N., Trenti, M., Santini, P., et al. 2022, arXiv e-prints, arXiv:2207.11135. <https://arxiv.org/abs/2207.11135>

Malkan, M. A., Cohen, D. P., Maruyama, M., et al. 2017, ApJ, 850, 5, doi: 10.3847/1538-4357/aa9331

Marchesini, D., Whitaker, K. E., Brammer, G., et al. 2010, ApJ, 725, 1277, doi: 10.1088/0004-637X/725/1/1277

Marchesini, D., Brammer, G., Morishita, T., et al. 2022, arXiv e-prints, arXiv:2207.13625 (Paper IX). <https://arxiv.org/abs/2207.13625>

Marsan, Z. C., Marchesini, D., Brammer, G. B., et al. 2015, ApJ, 801, 133, doi: 10.1088/0004-637X/801/2/133

Marsan, Z. C., Muzzin, A., Marchesini, D., et al. 2022, ApJ, 924, 25, doi: 10.3847/1538-4357/ac312a

McCarthy, P. J. 2004, ARA&A, 42, 477, doi: 10.1146/annurev.astro.42.053102.134032

McCarthy, P. J., Le Borgne, D., Crampton, D., et al. 2004, ApJL, 614, L9, doi: 10.1086/425306

Medezinski, E., Umetsu, K., Okabe, N., et al. 2016, ApJ, 817, 24, doi: 10.3847/0004-637X/817/1/24

Merlin, E., Fortuni, F., Torelli, M., et al. 2019, Monthly Notices of the Royal Astronomical Society, 490, 3309, doi: 10.1093/mnras/stz2615

Merlin, E., Bonchi, A., Paris, D., et al. 2022, ApJ Letters submitted, arXiv:2207.11701 (Paper II). <https://arxiv.org/abs/2207.11701>

Naidu, R. P., Oesch, P. A., van Dokkum, P., et al. 2022, arXiv e-prints, arXiv:2207.09434. <https://arxiv.org/abs/2207.09434>

Nedkova, K. V., H  u  ler, B., Marchesini, D., et al. 2021, Monthly Notices of the Royal Astronomical Society, 506, 928, doi: 10.1093/mnras/stab1744

Nonino, M., Glazebrook, K., Burgasser, A. J., et al. 2022, arXiv e-prints, arXiv:2207.14802 (Paper XIII). <https://arxiv.org/abs/2207.14802>

Rieke, G. H., Wright, G. S., B  ker, T., et al. 2015, Publications of the Astronomical Society of the Pacific, 127, 584, doi: 10.1086/682252

Rieke, M. J., Kelly, D., & Horner, S. 2005, in Society of Photo-Optical Instrumentation Engineers (SPIE) Conference Series, Vol. 5904, Cryogenic Optical Systems and Instruments XI, ed. J. B. Heaney & L. G. Burriesci, 1-8, doi: 10.1117/12.615554

Rigby, J., & et al. 2022, arXiv e-prints, arXiv:2207.05632. <https://arxiv.org/abs/2207.05632>

Roberts-Borsani, G. W., Ellis, R. S., & Laporte, N. 2020, MNRAS, 497, 3440, doi: 10.1093/mnras/staa2085

Schreiber, C., Glazebrook, K., Nanayakkara, T., et al. 2018, A&A, 618, A85, doi: 10.1051/0004-6361/201833070

Shipley, H. V., Lange-Vagle, D., Marchesini, D., et al. 2018, ApJS, 235, 14, doi: 10.3847/1538-4365/aaacce

Skelton, R. E., Whitaker, K. E., Momcheva, I. G., et al. 2014, ApJS, 214, 24, doi: 10.1088/0067-0049/214/2/24

Spitler, L. R., Straatman, C. M. S., Labb  , I., et al. 2014, ApJL, 787, L36, doi: 10.1088/2041-8205/787/2/L36

Steidel, C. C., Adelberger, K. L., Shapley, A. E., et al. 2003, The Astrophysical Journal, 592, 728

Straatman, C. M. S., Labb  , I., Spitler, L. R., et al. 2014, ApJL, 783, L14, doi: 10.1088/2041-8205/783/1/L14

Straatman, C. M. S., Spitler, L. R., Quadri, R. F., et al. 2016, ApJ, 830, 51, doi: 10.3847/0004-637X/830/1/51

Tomczak, A. R., Quadri, R. F., Tran, K.-V. H., et al. 2014, ApJ, 783, 85, doi: 10.1088/0004-637X/783/2/85

Treu, T., Roberts-Borsani, G., Bradac, M., et al. 2022, ApJ, in press, arXiv:2206.07978. <https://arxiv.org/abs/2206.07978>

Whitaker, K. E., Labb  , I., van Dokkum, P. G., et al. 2011, ApJ, 735, 86, doi: 10.1088/0004-637X/735/2/86

Wuyts, S., van Dokkum, P. G., Franx, M., et al. 2009, ApJ, 706, 885, doi: 10.1088/0004-637X/706/1/885

Yan, H., Ma, Z., Ling, C., et al. 2022, arXiv e-prints, arXiv:2207.11558. <https://arxiv.org/abs/2207.11558>

Zavala, J. A., Buat, V., Casey, C. M., et al. 2022, arXiv e-prints, arXiv:2208.01816. <https://arxiv.org/abs/2208.01816>